Eccentric strength and design of RC columns strengthened with SCC filled steel tubes

Yi-Yan Lu [*], Hong-Jun Liang [a], Shan Li [b] and Na Li [c]

School of Civil Engineering, Wuhan University, Wuhan City, Hubei Province, 430072, China

Abstract.   Self-compacting Concrete Filled steel Tubes (SCFT), which combines the advantages of steel and concrete materials, can be applied to strengthen the RC columns. In order to investigate the eccentric loading behavior of the strengthened columns, this paper presents an experimental and numerical investigation on them. The experimental results showed that the use of SCFT is interesting since the ductility and the bearing capacity of the RC columns are greatly improved. And the performance of strengthened columns is significantly affected by four parameters: column section type (circular and square), wall thickness of the steel tube, designed strength grade of strengthening concrete and initial eccentricity. In the numerical program, a generic fiber element model which takes in account the effect of confinement is developed to predict the behavior of the strengthened columns subjected to eccentric loading. After the fiber element analysis was verified against experimental results, a simple design formula based on the model is proposed to calculate the ultimate eccentric strength. Calibration of the calculated results against the test results shows that the design formula closely estimates the ultimate capacities of the eccentrically compressed strengthened columns by 5%.

Keywords: RC columns; strengthening; concrete-filled steel tube (CFT); eccentric strength

1. Introduction

Concrete-filled steel tube (CFT) column, which consists of a steel tube filled with concrete, has been widely used in modern building construction. It is mainly because the composite structure combines steel and concrete materials, resulting in a member that has the beneficial qualities of both materials (Elremaily and Azizinamini 2002). The former have the advantages of high tensile strength and ductility, while the latter are economical and have the advantages of high compressive strength and stiffness. The enhanced mechanical properties of CFT columns owe to the interaction of the steel tube and concrete. Due to the discrepancy of Poisson's ratios between concrete and steel, the expansion of the concrete core is confined by the exterior steel tube (Lu *et al.* 2007). Consequently, the concrete core is subjected to triaxial stress, and thereby the strength is enhanced

*Corresponding author, Ph.D. Professor, E-mail: yylu901@163.com
[a] Ph.D. Student, E-mail: hongjunliang8@163.com
[b] Ph.D. Professor, E-mail: lsdlut@163.com
[c] Ph.D. Student, E-mail: ln950228@163.com

and the deformation is confined. Meanwhile the presence of concrete infill prevents the steel tube from local buckling. As the excellent performance, the CFT has the potential to be used to strengthen RC columns.

Some research projects have been conducted to investigate the behaviors of RC columns strengthened with CFT. Priestley *et al.* (1994a, b) proposed the method of square RC columns strengthened with concrete-filled elliptical steel tubes (CFET) and performed a shear test on them. The test results indicated that the lateral stiffness of the strengthened columns was increased by an average of 64% and the ductility was significantly improved. Nevertheless, the elliptical tube would result in substantial changes in the section of the columns. Thus it may not be favorable for repairing rectangular or square columns perfectly from the architectural and functional points of view. Miller (2006) and Sezen (Sezen and Miller 2011) conducted axial loading tests on circular RC columns strengthened with concrete-filled circular steel tube (CFCT). Compared with the experimental results of concrete jacket and FRP jacket strengthening methods, CFCT strengthening method is more effective to improve the specimen stiffness, member strength and ductility because of the existence of sufficient confinement. Meanwhile section size of the columns can be reduced to provide more useable floor. Furthermore, CFCT strengthening method requires less construction time and costs because the tube instead of hoop and longitudinal reinforcements and can serve as formwork. Wang (2011) studied the axial loading behavior of the RC columns with- and without initial stress conditions strengthened with concrete-filled circular steel tubes (CFCT). It was reported that the CFCT can not only improve the axial bearing capacity but also improve the ductility greatly. Moreover, the initial stress had less influence on the ultimate bearing capacity of the strengthened columns while had some adverse impact on the ductility. Zhou *et al.* (2012) conducted axial loading tests on 6 circular RC columns strengthened with CFCT. They reported that the constraint function of steel tube on the internal concrete is obvious and the confinement effect becomes more obvious with the increase of wall thickness. However, it has been found from the above research that the gap between the formwork (steel tubes) and RC columns is so narrow that the formwork cannot be filled uniformly by Normal Vibrated concrete (NVC). Consequently, the columns displayed many surface voids from the improper compaction cover after the formwork was removed. It seriously reduced the bond strength to make the confinement ineffective. Therefore, Lu *et al.* (2013) improved the technology of concrete pouring. Self-Compacting Concrete (SCC) which allows pouring concrete easily without vibration even in the presence of a highly dense reinforcement or novel form of construction (Muciaccia *et al.* 2011, Holschemacher *et al.* 2004) has been filled in the gap. However SCC displayed higher shrinkage than NVC due to the higher volume of paste (Loser and Leemann 2009), it will not only make poor concrete-steel interface bond strength but even deteriorate their interaction due to local separation (Roeder *et al.* 1999). To overcome this deficiency, the right amount of concrete expansion agent has been added to compensate for the shrinkage of SCC and enhance the bond strength (Chang *et al.* 2009). The experimental results demonstrated that the concrete cover is properly compacted.

As described above, the CFT strengthening method is effective to improve the stiffness, member strength and ductility of RC columns with less construction time and cost, and the use of SCC can improve the technology of concrete pouring. However, some issues concerning the mechanical properties of member material and the design method of the ultimate strength under eccentric load still remain unsolved. Therefore, this paper performs an experimental and numerical investigation on the behavior of RC columns strengthened with self-compacting concrete filled steel tubes (SCFT) subjected to eccentric load. In the experimental program, 16 column specimens

were tested under the eccentric load. The failure mode, the ultimate eccentric strengths and the deflection at mid-height are investigated. In the numerical program, a generic fiber element model which takes in account the effect of confinement is developed to predict the behavior of the strengthened columns subjected to eccentric load, and subsequently a simple design formula based on the verified model is proposed.

2. Experimental program

2.1 Test specimens

In this experimental program, 16 specimens were tested under eccentric compression loading including 1 square RC columns without strengthening (WSRC), 1 circular RC columns without strengthening (WCRC), 7 square RC columns strengthened with self-compacting concrete filled square steel tubes (SRC), and 7 circular RC columns strengthened with self-compacting concrete filled circular steel tubes (CRC). The strengthening procedure is to strip off the protective layer and deficient section of RC column firstly, when necessary, and then pack a circular (for circular sections) or a square (for square sections) steel tube jacket welded by two pieces of semicircular or L-shaped steel plates, and pour in the strengthening concrete lastly to make them work together. The cross section details of all the specimens are shown in Fig. 3. The main parameters for the tests are as follows: (1) column section type, which has circular and square; (2) the nominal wall thickness of steel tubes (t), which includes 2 mm, 3 mm, 4 mm; (3) the designed strength grade of strengthening concrete (C), C40, C50 and C60 were chosen; (4) initial eccentricity (e_0), which

(a) WCRC
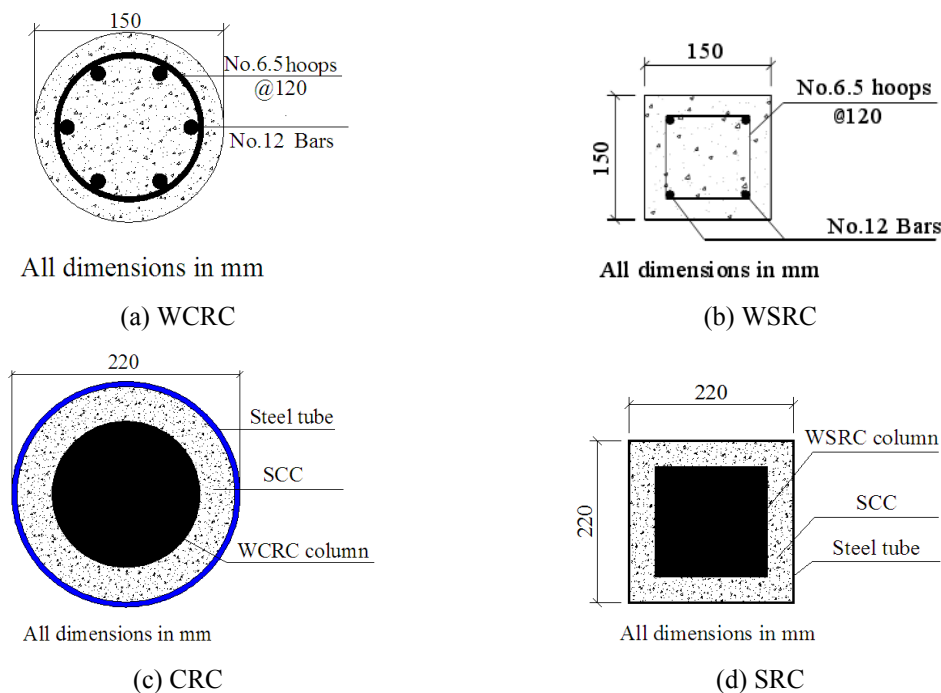
(b) WSRC

(c) CRC

(d) SRC

Fig. 1 Cross section of the specimens

changes from 15 to 45 mm. All the test parameters for each specimen are summarized in Table 1, where D is dimension of circular cross-section, B is width of square cross-section, L which stands the height of columns is set 720 mm. The nomenclature followed in the tests is: XRCt-C-e_0 (i.e., SRC3-C50-e30), where X stands for column section type.

2.2 Material properties

The RC columns were reinforced with four 12mm diameter longitudinal bars, and were transversely reinforced with 6.5 mm diameter hoops, spaced at 120 mm. Two pieces of semicircular or L-shaped steel plates, accurately cut and machined to the required length and thickness, were butt welded into the square steel jacket. Tensile tests on the coupons taken from the steel plates and reinforcement were conducted to measure steel material properties. The average yield strength (f_y) of the steel, the modulus of elasticity (E_s) and elongation rate obtained from the tests are shown in Table 2. As model columns simulating deficient columns, the RC columns were poured with NVC whose nominal compressive strength was low to 25 MPa. The design strength grade of the SCC varied between 40, 50 and 60 MPa. The actual concrete compressive strength f_{cu} was determined by testing cube specimens of dimensions $150 \times 150 \times 150$ mm after 28 days of curing. f_c is the prism compressive strength ($f_c = 0.67 f_{cu}$) and f_c' is the

Table 1 Geometrical and material parameters for all test specimens

Section type	Specimen	$D(B) \times t \times L$ /mm	Concrete grade	Initial eccentricity e_0 /mm	N_{exp} / kN	N_{fib} / kN	N_{fib} / N_{exp}	N_{pre} / kN	N_{pre}/ N_{exp}
Circular	WCRC-C25	150×0×720	C25	30	390	-	-	-	-
	CRC2-C50-e30	220×2×720	C50	30	1720	1650	0.96	1835	1.07
	CRC3-C50-e30	220×3×720	C50	30	2010	1918	0.95	1874	0.93
	CRC4-C50-e30	220×4×720	C50	30	2290	2031	0.89	1956	0.85
	CRC3-C40-e30	220×3×720	C40	30	1940	1834	0.95	1734	0.89
	CRC3-C60-e30	220×3×720	C60	30	2050	1960	0.96	2009	0.98
	CRC3-C50-e15	220×3×720	C50	15	2490	2266	0.91	2084	0.84
	CRC3-C50-e45	220×3×720	C50	45	1760	1608	0.91	1703	0.97
Square	WSRC-C25-e30	150×0×720	C25	30	430	-	-	-	-
	SRC2-C50-e30	220×2×720	C50	30	1670	1538	0.92	1745	1.04
	SRC3-C50-e30	220×3×720	C50	30	1800	1847	1.03	1790	0.99
	SRC4-C50-e30	220×4×720	C50	30	2000	1987	0.99	1892	0.95
	SRC3-C40-e30	220×3×720	C40	30	1710	1736	1.02	1735	1.01
	SRC3-C60-e30	220×3×720	C60	30	1880	1847	0.98	1942	1.03
	SRC3-C50-e15	220×3×720	C50	15	2030	2024	1.00	2042	1.01
	SRC3-C50-e45	220×3×720	C50	45	1570	1561	0.99	1593	1.01
Mean							0.96		0.97
Standard deviation (SD)							0.041		0.067
Coefficient of variation (COV)							0.042		0.069

Table 2 Material properties of steel

Steel	t or D (mm)	f_y / MPa	Es / GPa	Elongation rate / %
	1.78	307.1	202	22
Steel tube	2.80	280.3	205	25
	3.80	265.2	209	28
Hoop reinforcements	6.5	310.4	189	25
Longitudinal reinforcements	12	384.2	195	22

Table 3 Mix proportions (kg/m^3) and compressive strength of concrete (MPa)

Concrete grade	Water	42.5R cement	River Sand	Coarse aggregate	Expansive agent	Water reducer	Fly ash	f_{cu}	f_c	f_c'
C25 NVC	218.8	336.7	733.9	1198.5	-	-	-	32.6	21.8	26.5
C40 SCC	184.7	432.5	784.5	953.2	1.7	48.0	83.5	48.8	32.7	38.8
C50 SCC	193.9	484.7	737.7	927.3	1.9	49.4	95.0	52.1	34.9	42.1
C60 SCC	179.0	487.8	715.6	969.7	2.0	48.0	92.7	61.1	40.9	50.8

(a)   (b)

Fig. 2 Details of setup and instrumentation

cylinder compressive strength equivalent translated by Eurocode 2. All of these are summarized in Table 3.

2.3 Test setup and instrumentation layout

All the specimens were tested with a 5,000 kN capacity universal testing machine. Fig. 2 gives the schematic view of the test setup and instrument layout. In the tests, the eccentric load was applied through a triangular hinge to simulate a desired pinned support, which allows the specimen

to rotate but restrains its translation at the same time. The male edge was placed at the center of the testing machine. Then, the female edge was positioned onto the male edge according to the required load eccentricity. A force transducer was placed below the bottom to accurately measure the applied axial load in real-time. Three linear variable displacement transducers (LVDTs) were used to symmetrically measure the deflection of the column at the mid-height (0.5 L) and quarter-heights (0.25 L, 0.75 L). A computerized data-acquisition system was used to collect the experimental data of the load and deflection.

3. Experimental results and analysis

3.1 Failure mode

Two types of failure modes including the material failure and the outward local buckling of steel tubes were observed in this experiment as shown in Fig. 3. For the WRC columns, the typical failure mode was the material failure as shown in Fig. 3(a). The cover concrete was spalling and flaking and the longitudinal reinforcements were serious buckling coincided with the failure of the specimen. For SRC columns, the tested stub columns behaved in a relatively ductile manner. The typical failure mode was the outward local buckling of steel tubes because of the stability supplied by the infill of SCC concrete as shown in Figs. 3(b)-(c). The local buckling was observed between the quarter height and the mid-height of the specimens. When the test terminated, several obvious bulges were observed along the height.

3.2 Ultimate eccentric strengths

The experimental ultimate strengths of the strengthened columns are shown in Fig. 4. For convenience of comparison, all tested columns are divided into several series. From the figure, the following conclusions are reached within the scope of the current research:
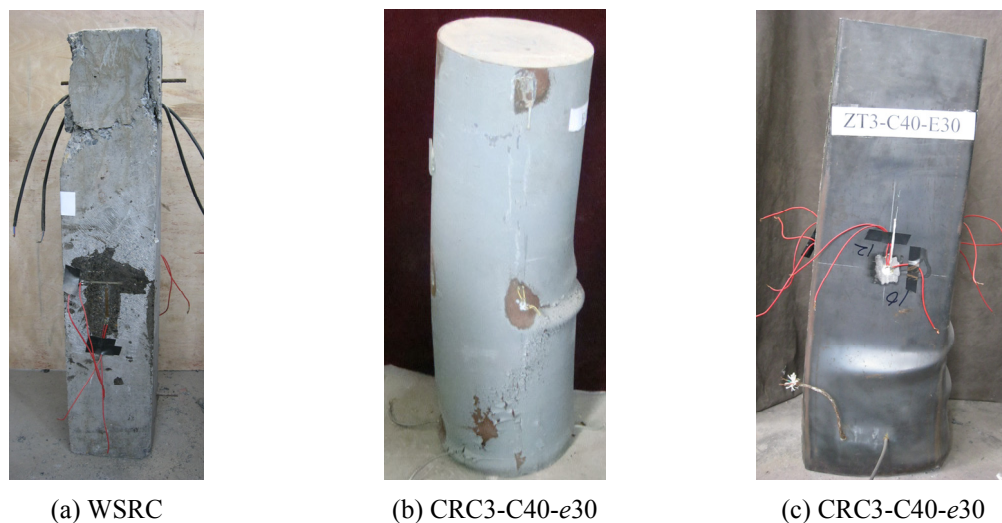

| (a) WSRC | (b) CRC3-C40-*e*30 | (c) CRC3-C40-*e*30 |

Fig. 3 Typical failure modes of the tested columns

(1) For WRC columns, as we expected, square cross-section column (represented by red columns in Fig. 4) with larger cross-section area has a higher load carrying capacity than circular cross-section column (represented by black columns). However, the eccentric load carrying capacity of SRC columns with larger cross-section is approximate 12% less than that of CRC columns, which indicates that the enhanced confinement provided by circular steel tube is more effective than that of square steel tubes.

(2) The wall thickness of steel tubes has a significant effect on the ultimate eccentric strength of strengthened columns. The ultimate strength significantly increases as the wall thickness is increased. The ultimate strength of CRC3-C50-e30, CRC4-C50-e30 are 16.9% and 33.1% respectively more than that of CRC2-C50-e30, while the ultimate strength of SRC3-C50-e30, SRC4-C50-e30 are 7.8% and 19.8% respectively more than that of SRC2-C50-e30.

(3) The ultimate strength slightly increases as the concrete strength is increased. The ultimate strength of CRC3-C50-e30, CRC3-C60-e30 are 3.6% and 5.7% respectively more than that of CRC3-C40-e30, while the ultimate strength of SRC3-C50-e30, SRC3-C60-e30 are 5.3% and 9.9% respectively more than that of SRC3-C40-e30.

(4) The initial eccentricity has a remarkably detrimental effect on ultimate strength of strengthened columns. The ultimate strength decreases considerably with an increase in the initial eccentricity. The ultimate strength of CRC3-C50-e30, CRC3-C50-e45 are 23.9% and 41.5% respectively less than that of CRC3-C50-e15, while the ultimate strength of SRC3-C50-e30, SRC3-C50-e45 are 12.8% and 29.3% respectively less than that of SRC3-C50-e15. In order to achieve the aims of safety, the strengthened columns with large initial eccentricity are not recommended to be used in practice.

3.3 Applied load (N)-lateral deflection at mid-height (f_m)

Fig. 5 presents the N-f_m curves measured by experiments for the RC columns with- and without strengthening. And the circular cross-section strengthened columns are placed on the left, while
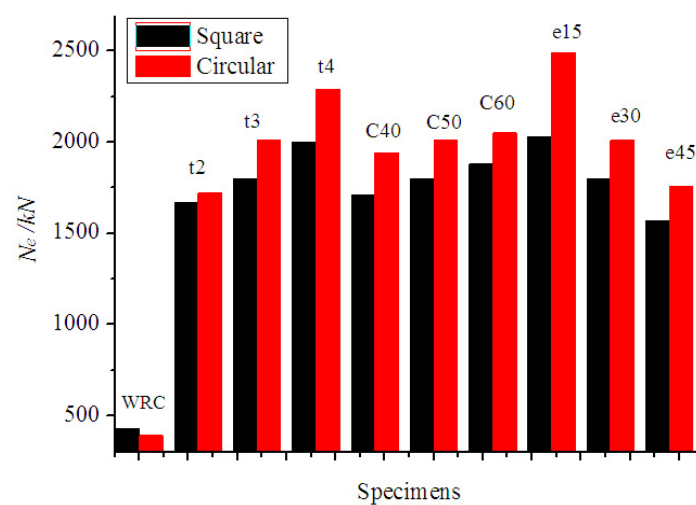

Fig. 4 The ultimate eccentric strengths of the tested columns

(a) Various wall thickness of steel tubes

(b) Various strengths of concrete

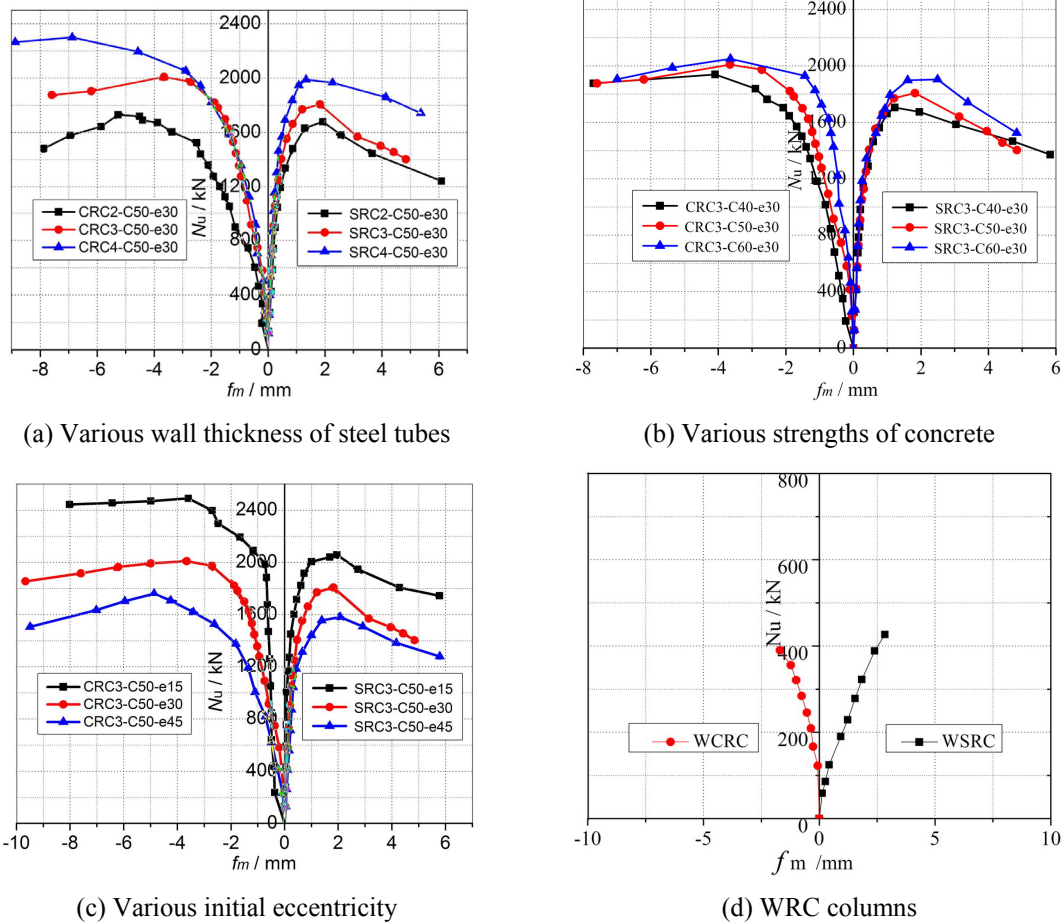(c) Various initial eccentricity

(d) WRC columns

Fig. 5 Applied load versus the deflection at the mid-height curves

the square columns are placed on the right. And in order to illustrate the interaction between steel and concrete during the loading, the applied load versus the Poisson's ratio of the strengthened columns is presented in Fig. 6. The Poisson's ratio is equal to the ratio of the lateral strain and longitudinal strain which are obtained by the strain gauges.

It can be seen that all the strengthened columns are in elastic stage and the curves are roughly linear growth in the early load. In this stage, the Poisson's ratio of the strengthened columns was a relatively stable value (about 0.24) as shown in Fig. 6. The value is approximately the Poisson's ratio of steel (about 0.25~0.30) and is greater than the Poisson's ratio of concrete (about 0.17~0.20). Thus, the lateral expansion of concrete is smaller than the steel tube under the same longitudinal deformation so that the steel tube has no confining effect on the concrete core at the initial stage of loading. So SRC columns exhibit more steep slope than CRC because the flexural stiffness (EI) of SRC columns section is about 1.7 ($= 16/3\pi$) times of CRC columns section under the condition of $D = B$. And as shown in Figs. 5(b)-(c), the difference of the EI also leads to the slope of curves increases with the concrete compressive strengths and the wall thickness of steel tubes increasing. However, CRC3-C50-e45 and SRC3-C50-e45 have a less steep slope in Fig. 5(c), although the
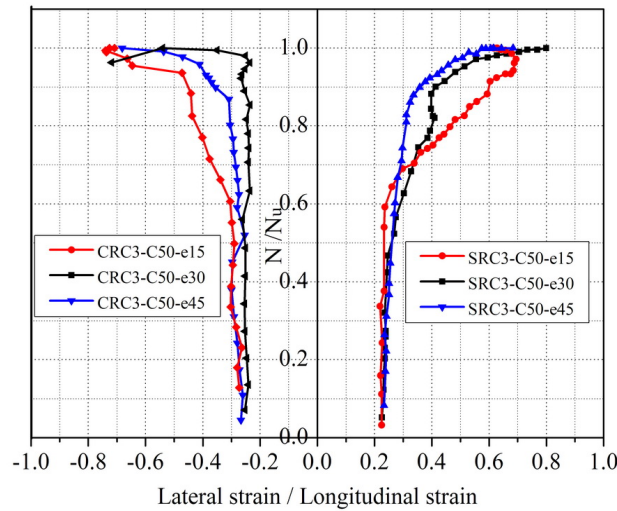
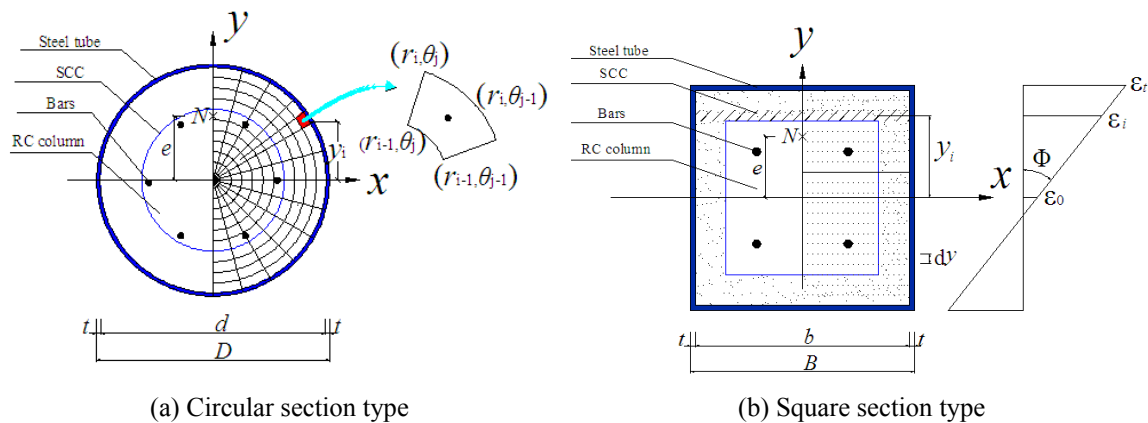Fig. 6 Applied load versus the Poisson's ratio of the strengthened columns

(a) Circular section type   (b) Square section type

Fig. 7 Strain distribution in strengthened column section

flexural stiffness is equal to others. It is because the larger initial eccentricity (e_0) will generate a greater bending moment under the same applied load so that the lateral deflection is larger than others. Subsequently, the steel tube gradually goes into elastic-plastic state, and its tangent modulus decreases significantly. The N-f_m curve diverges from its initial linearity. However the modulus of concrete decreases slightly at the same time so that the stress is redistributed between the steel tubes and the concrete persistently. The stress on the concrete increases significantly so that Poisson's ratio of concrete increases. Fig. 6 shows that the Poisson's ratio is larger than 0.3 even beyond 0.5 after the applied load is up to approximately 70% of the ultimate load. The lateral expansion of the concrete core gradually catches up with that of steel. Therefore, a radial stress develops at the steel–concrete interface, which causes the concrete core to be subjected to triaxial stress, thereby enhancing the concrete strength and confining the deformation. It can be surprisedly seen in Fig. 5 that the CRC columns curves possess longer elastic-plastic stage than

SRC and higher ultimate bearing capacity, which also indicates the enhanced confinement provided by circular steel tube is more effective than that of square steel tube. After the ultimate strength, the strengthened columns enter the failure stage. The applied load needs to be decreased persistently in order to keep counterbalance. However the applied load is still kept constant at a certain loading level because of the good ductility caused by the effective confinement of steel tubes. Compared with Fig. 5(d), Figs. 5(a)-(c) indicate that the use of SCFST is interesting since the ductility and the bearing capacity of the RC columns are greatly improved, and the CRC columns have a better ductility than SRC columns. Meanwhile, the ductility significantly increases with the wall thickness of steel tubes increasing. And the ductility significantly decreases with the strength increasing, especially in the use of high strength concrete (i.e., SRC3-C60-e30).

4. Fiber element analysis

4.1 Fiber element discretization

The fiber element analysis method is a simple and yet efficient numerical technique for predicting the ultimate strengths of composite columns (Lu *et al*. 2007, Wang *et al*. 2000, Liu 2006 and Liang 2011). In the fiber element method, the concrete and the steel need to be discretized into a number of elements as depicted in Fig. 7. The more elements we discretize, the more accurate prediction will be obtained. In the analysis, it is assumed that there is no slippage between the strengthened section and the RC column so that the cross section remains plane, and the steel tube and the concrete deform compatibly when the column deflects, resulting in a linear strain distribution. Therefore, the strain for the centroidal area of the element *i* is calculated as

$$\varepsilon_i = \varepsilon_0 + \Phi y_i \tag{1}$$

where ε_0 is the strain at the centroid axis of the cross section, Φ is the curvature of the column and y_i is the coordinate of the fiber element.

4.2 Material constitutive models

4.2.1 Steel
In the analysis, the stress–strain relation for steel is in the following form (see Fig. 8(a))

$$\sigma_s = \begin{cases} f_y & (\varepsilon \geq \varepsilon_y = f_y / E) \\ \varepsilon E & (-\varepsilon_y \leq \varepsilon < \varepsilon_y) \\ -f_y & (\varepsilon < -\varepsilon_y) \end{cases} \tag{2}$$

where f_y, E and ε_y are the yield stress, the elastic modulus and the yield strain of steel respectively.

4.2.2 Concrete modeling
In the analysis, the tensile strength of concrete is negligible. For the concrete in compression, Eq. (3) (Han 2007) is proposed to determine the triaxial stress-strain relationship for concrete core considering the confinement provided by the steel tube. Shown in Fig. 8(b) is the typical σ-ε curve

for the confined concrete. It is found that the σ-ε curve has a descent stage after the strain exceeds ε_0 when $\xi < \xi_0$ while the stress keeps constant at a certain level when the confinement factor is large enough $\xi \geq \xi_0$.

$$
\frac{\sigma}{\sigma_0} = \begin{cases} 2\left(\dfrac{\varepsilon}{\varepsilon_0}\right) - \left(\dfrac{\varepsilon}{\varepsilon_0}\right)^2 & (\varepsilon \leq \varepsilon_0) \\[4mm] \dfrac{\dfrac{\varepsilon}{\varepsilon_0}}{\beta\left(\dfrac{\varepsilon}{\varepsilon_0} - 1\right)^{\eta} + \dfrac{\varepsilon}{\varepsilon_0}} & (\varepsilon > \varepsilon_0) \end{cases}
\tag{3}
$$

For circular sectional steel tube, where

$$
\left.\begin{aligned}
\sigma_0 &= \left[1 + (-0.054\xi^2 + 0.4\xi)\left(\frac{24}{f_c'}\right)^{0.45}\right] f_c' \\[2mm]
\varepsilon_0 &= 1300 + 12.5 \cdot f_c' + \left[1400 + 800\left(\frac{f_c'}{24} - 1\right)\right]\xi^{0.2} \\[2mm]
\eta &= 2 \\[2mm]
q &= \frac{\xi^{0.745}}{2 + \xi} \\[2mm]
\beta &= (23.6 \times 10^{-5})^{[0.25 + (\xi - 0.5)^7]} \cdot f_c'^2 \cdot 3.51 \times 10^{-4}
\end{aligned}\right\}
\tag{4}
$$

For square sectional steel tube, where

$$
\left.\begin{aligned}
\sigma_0 &= \left[1 + (-0.0135\xi^2 + 0.1\xi)\left(\frac{24}{f_c'}\right)^{0.45}\right] f_c' \\[2mm]
\varepsilon_0 &= 1300 + 12.5 \cdot f_c' + \left[1330 + 760\left(\frac{f_c'}{24} - 1\right)\xi^{0.2}\right](\mu\xi) \\[2mm]
\eta &= 1.6 + \frac{1.5\varepsilon_0}{\varepsilon} \\[2mm]
\beta &= \begin{cases} \dfrac{(f_c')^{0.1}}{1.35\sqrt{1 + \xi}} & (\xi \leq 3.0) \\[4mm] \dfrac{(f_c')^{0.1}}{1.35\sqrt{1 + \xi}(\xi - 2)^2} & (\xi > 3.0) \end{cases}
\end{aligned}\right\}
\tag{5}
$$

in which $\xi = A_{s2}f_{y2}/(A_{c1}f_{ck1} + A_{c2}f_{ck2})$, A_{s2}, f_{y2} are the cross-sectional area and the yield stress of steel

(a) Steel   (b) Confined concrete
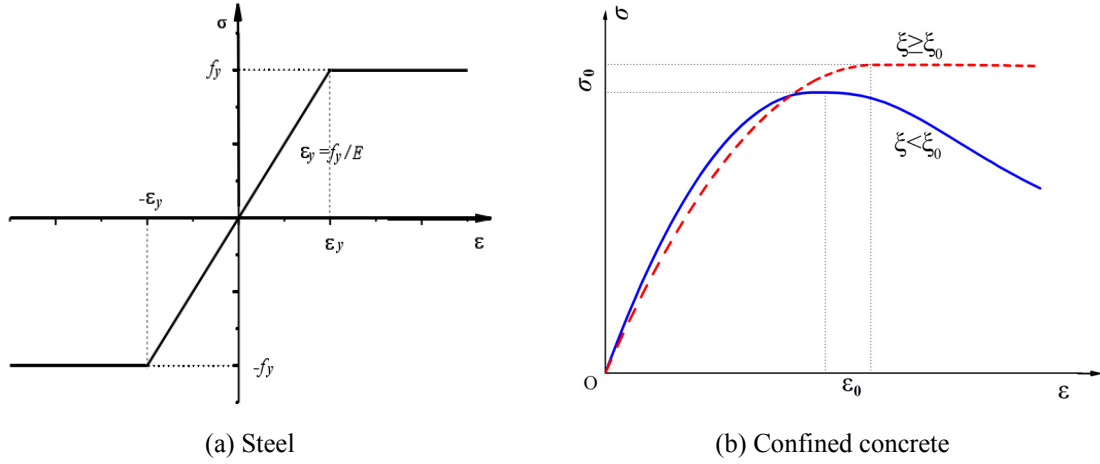
Fig. 8 The stress-strain relation for the steel and the confined concrete

tube, A_{c1} and A_{c2} are the cross-sectional area of RC column concrete and strengthening concrete, f_{ck1} and f_{ck2} are the nominal strength of RC column concrete and strengthening concrete. f_c' was the cylinder compressive strength of concrete.

4.3 Equilibrium equations

The stresses of steel and concrete in the finite strip can thus be determined based on the strain and respective constitutive relationships. Based on the areas and stresses of the steel and concrete, the applied load and the bending moment acting on the composite section can be determined as in Eqs. (6) and (7), respectively.

$$N = \sum (\sigma_{c1i}dA_{c1i} + \sigma_{c2i}dA_{c2i} + \sigma_{s2i}dA_{s2i} + \sigma_{s2i}dA_{s2i}) \tag{6}$$

$$M = \sum (\sigma_{c1i}y_idA_{c1i} + \sigma_{c2i}y_idA_{c2i} + \sigma_{s2i}y_idA_{s2i} + \sigma_{s2i}y_idA_{s2i}) \tag{7}$$

where σ_{c1i}, σ_{c2i}, σ_{s1i} and σ_{s2i} are the longitudinal stresses at the centroid of RC column concrete, strengthening concrete, steel bars and steel tube fiber i, respectively. A_{c1i}, A_{c2i}, A_{s1i}, A_{s2i} are the cross-sectional area of RC column concrete, strengthening concrete, steel bars and steel tube fiber i. y_i is the coordinates of fiber i.

The simplified calculation model is schematically depicted in Fig. 9. In this figure, it is approximately considered that the equilibrium is maintained at the mid-height of the compressed column. The deflected shape (f) of the compressed column is assumed to be a half sine-wave and consequently expressed by

$$f = f_m \sin\left(\frac{\pi z}{L}\right) \tag{8}$$

where f_m is the deflection at the mid-height of the column and L is the effective length of the column.

The curvature (Φ) at the mid-height of the columns can be obtained from Eq. (9) as

$$\Phi = \frac{\partial^2 f}{\partial z^2}\bigg|_{z=\frac{L}{2}} = \left(\frac{\pi}{L}\right)^2 f_m \sin\left(\frac{\pi z}{L}\right)\bigg|_{z=\frac{L}{2}} = \left(\frac{\pi}{L}\right)^2 f_m \tag{9}$$

The external bending moment at the mid-height section of the columns under eccentric loading can be calculated by

$$M = N(e_0 + f_m) \tag{10}$$

Where N is the applied load and e_0 is the initial eccentricity of the applied load.

In Eqs.(6)-(10) , ε_0, Φ, M, f, f_m, N are unknown variables to be solved. Thus N-f_m relation for a strengthened column under a certain initial eccentricity e_0 is determined. As the calculation process is more complicated, a computational algorithm needs to be developed. The main steps of the computational procedure are given as

(1) Input date.
(2) Discretize the composite section into fiber elements.
(3) Set initial deflection ($f_m = 0.05$ mm) at the mid-height of the strengthened columns.
(4) Calculate the curvature Φ at the mid-height of the strengthened columns using Eq. (9).
(5) Set $\varepsilon_0 = 2(\mu\varepsilon)$
(6) Calculate the strain (ε) and the stress (σ) for element i using Eqs. (1)-(3).
(7) Compute the axial load N and moment M using Eqs. (6)-(7).
(8) If $\left|\dfrac{M}{N} - f - e_0\right| > \Delta$, increase the $\varepsilon_0 = \varepsilon_0 + 2$.

(9) Repeat steps (6)-(8) until $\left|\dfrac{M}{N} - f - e_0\right| \leq \Delta$, record the value of M and N.

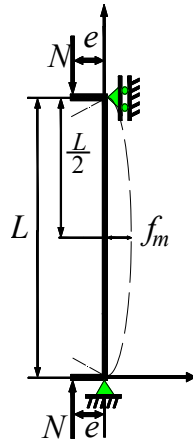(10) Increase the deflection ($f_m = f_m + 0.05$) at the mid-height of the strengthened columns and repeat steps (4)-(9) until $f \leq$ limit.
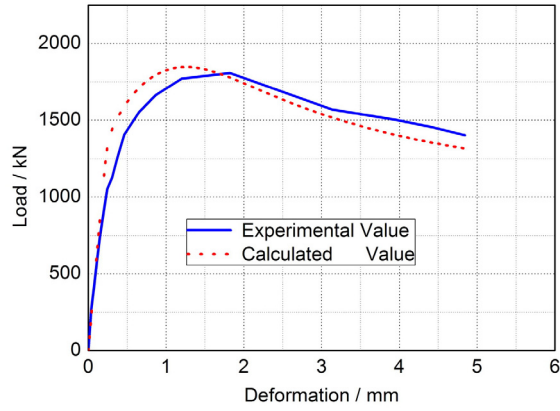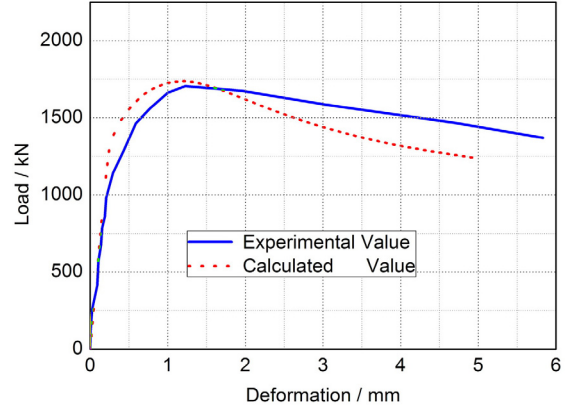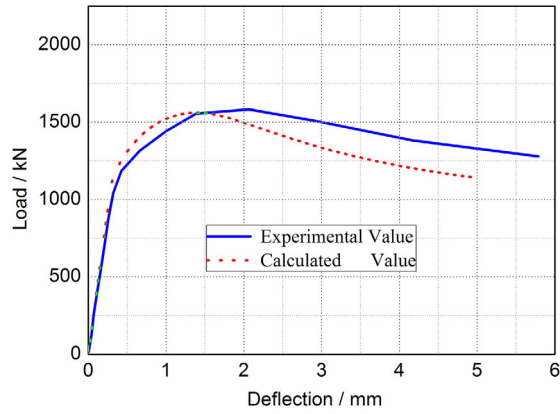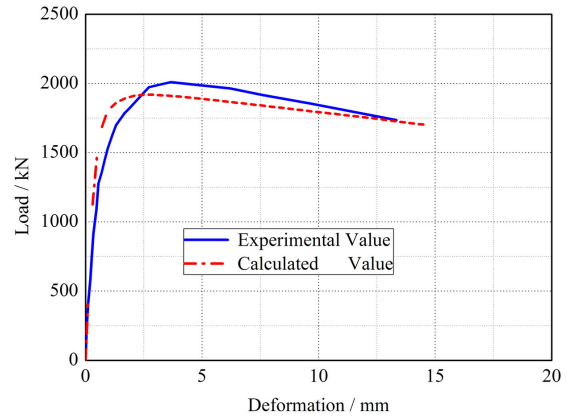

Fig. 9 Pin-ended compressed columns model
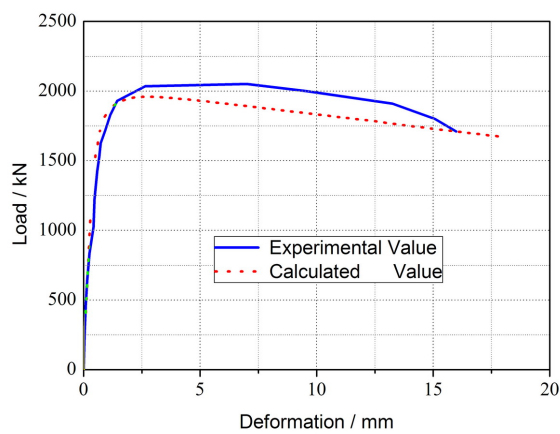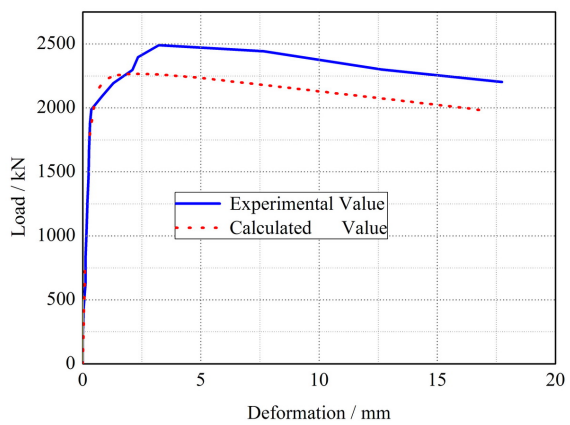
(a) SRC3-C50-e30

(b) SRC3-C40-e30

(c) SRC3-C50-e45

(d) CRC3-C50-e30

(e) CRC3-C60-e30

(f) CRC3-C50-e15

Fig. 10 Comparison of predicted and experimental applied load versus the deflection at the mid-
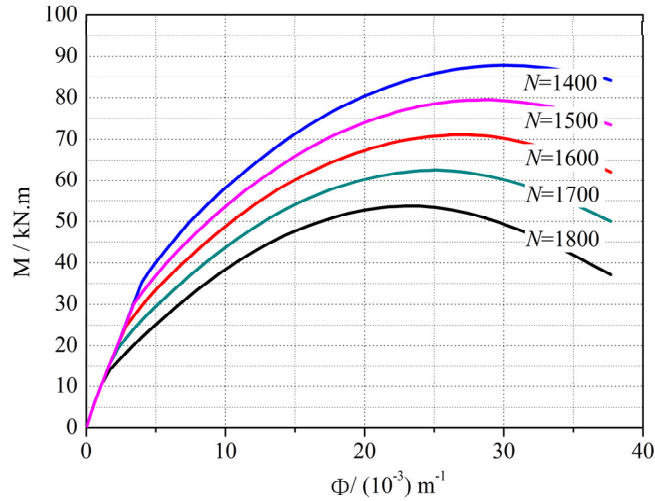height curves of the eccentrically compressed columns

Fig. 11 The *M*-Φ curve of the square cross-section under different applied loads

The convergence tolerance Δ is set to 10^{-3} in the analysis. The computational procedure will predict the complete load-deflection response and the ultimate strengths of the strengthened columns under eccentric loads. The N-f_m curves calculated by numerical studies for the strengthened columns are shown in Fig. 10 and the ultimate strengths are listed in Table 1, where N_{exp} is denoted as the experimental ultimate axial load and N_{fib} is denoted as the ultimate axial load predicted by the fiber element analysis.

From the comparisons of N-f_m interaction curve, it can be found that the test results and predicted results by the fiber element analysis are generally good agreement, especially in the ascent stage. However, at the descent stage, the predicted load is larger obviously than experimental applied loads for the same deflection. The reason is probably that the cross section cannot remain plane at the failure stage so that Eq. (1) cannot be established. Fortunately, it does not affect the following analysis of the ultimate strength. Moreover, it can be seen from the Table 1 that the fiber element analysis technique gives very good prediction of the ultimate strengths of strengthened columns. The mean ultimate eccentric strength predicted by the fiber element analysis technique is 0.96 of the experimental value. The standard deviation (SD) of N_{fib}/N_{exp} is 0.041 while its coefficient of variation (COV) is 0.036. It indicates that the fiber element analysis model can give accurate prediction of the strengthened columns under eccentric load and can be used to conduct further analysis.

5. Simplified formula

In Eqs. (6)-(10), the *M*-Φ relation for the strengthened columns under a certain axial load *N* can also be determined by the aforementioned computational procedure. Fig. 11 presents the *M*-Φ curves for a typical square cross-section strengthened columns. The curve can be divided into two stages: ascent stage and the descent stage. The ascent stage of *M*-Φ curve resembles a parabola. It can also been derived from the above Equations. Based on simultaneous Eqs. (9) and (10), we can have

$$M = Ne_0 + \left(\frac{L}{\pi}\right)^2 N\Phi \tag{11}$$

It is found that the bending moment (*M*) is proportional to the applied load (*N*). Furthermore from the analysis of the Section 3.3, the ascent stage (the elastic stage and the elastic-plastic stage) of *N-f_m* curve can resemble a straight line in order to simplify calculation. Therefore, the applied load (*N*) is approximately proportional to the curvature (Φ) at the mid-height of the columns based on the Eq. (9). Consequently, the ascent stage of *M*-Φ curve is simplified as a parabola and the bending moment (*M*) can be expressed as

$$M = \left[2\frac{\Phi}{\Phi_0} - \left(\frac{\Phi}{\Phi_0}\right)^2\right]M_u \qquad (\Phi \leq \Phi_0) \tag{12}$$

where Φ_0 is the curvature when the bending moment *M* reaches M_u. Based on the results of numerical and experimental calculation, an empirical Equation is proposed for Φ_0

$$\Phi_0 = \begin{cases} \dfrac{2}{\sqrt{3}} \cdot \dfrac{4.0f_y}{ED} & \text{(For circular section)} \\[3mm] \dfrac{4.0f_y}{EB} & \text{(For square section)} \end{cases} \tag{13}$$

So we have

$$M = N\left(e_0 + \left(\frac{L}{\pi}\right)^2 \Phi\right) = \left[2\frac{\Phi}{\Phi_0} - \left(\frac{\Phi}{\Phi_0}\right)^2\right]M_u \qquad (\Phi \leq \Phi_0) \tag{14}$$

And then, it is seen from Eq. (10) that the bending moment (*M*) does not reach the ultimate bending moment M_u before the applied load (*N*) reaches the ultimate load (N_u). Therefore to get N_u, we take the derivative with respect to Φ and let $dN / d\Phi = 0$, and then have

$$N\left(\frac{L}{\pi}\right)^2 = 2M_u\frac{\Phi_0 - \Phi}{\Phi_0^2} \tag{15}$$

Substitute Eq. (14) into above Equation, we have

$$\Phi = \Phi_0 k(\sqrt{1 + 2/k} - 1) \tag{16}$$

where

$$k = \frac{e_0\pi^2}{\Phi_0 L^2} \tag{17}$$

Substitute Eqs. (16) and (17) into Eq. (14) gives the ultimate load (N_u) as

$$N_u = \frac{2M_u k}{e_0}(1 + k - \sqrt{k^2 + 2k})$$ (18)

Therefore, if we want to obtain N_u, we just require the solution of M_u. As discussed above, the ultimate bending moment M_u can be obtained by the aforementioned method for a certain eccentric load. By repeating this process, a set of applied loads and the corresponding ultimate moments will be obtained. The relation between M_u and N is plotted as a M_u-N interaction curve as shown in Fig. 12. According to the characteristic of M_u-N curve, the curve is assumed to be piece-wisely linearized in order to simplify calculation in this paper. Based on the results of numerical calculation and the expression formulas of M_u-N interaction curve for the CFST columns proposed by Han (2007), the M_u-N interaction for the strengthened columns when $0.2 < \xi < 5$ are expressed as

$$M_u \approx \begin{cases} \dfrac{M_{SC}}{aN_{SC}}(N_{SC} - N) & (N > N_C) \\[2mm] M_{SC} & (N \leq N_C) \end{cases}$$ (19)

For circular sectional steel tube, where

$$\left. \begin{aligned} & M_{SC} = \gamma_m W_{scm} f_{scy} + W_{s1} f_{s1} \\ & \gamma_m = 1.34 + 0.48\ln(\xi + 0.1) \\ & f_{scy} = (1.18 + 0.85\xi) \cdot f_{ck} \\ & f_{ck} = (f_{ck1}A_{c1} + f_{ck2}A_{c2})/(A_{c1} + A_{c2}) \\ & a = 0.8 - 0.22\xi^{-0.81} \\ & N_{SC} = f_{scy} \cdot (A_{c1} + A_{c2} + A_{s2}) + f_{y1}A_{s1} \\ & N_C = N_{SC}(1 - a) \end{aligned} \right\}$$ (20)

For square sectional steel tube, where

$$\left. \begin{aligned} & M_{SC} = \gamma_m W_{scm} f_{scy} + W_{s1} f_{s1} \\ & \gamma_m = 1.1 + 0.48\ln(\xi + 0.1) \\ & f_{scy} = (1.14 + 1.02\xi) \cdot f_{ck} \\ & f_{ck} = (f_{ck1}A_{c1} + f_{ck2}A_{c2})/(A_{c1} + A_{c2}) \\ & a = 0.8 - 0.36\xi^{-0.81} \\ & N_{SC} = f_{scy} \cdot (A_{c1} + A_{c2} + A_{s2}) + f_{y1}A_{s1} \\ & N_C = N_{SC}(1 - a) \end{aligned} \right\}$$ (21)

in which M_{sc} is ultimate bending moment under pure bending, N_{sc} is the ultimate strength of the strengthened columns under axial load. The simplified typical M_u–N interaction curve and the actual typical M_u–N interaction curve are shown in Fig. 12. It is found that close agreement is achieved between them, especially in the stage of $M < M_{sc}$.
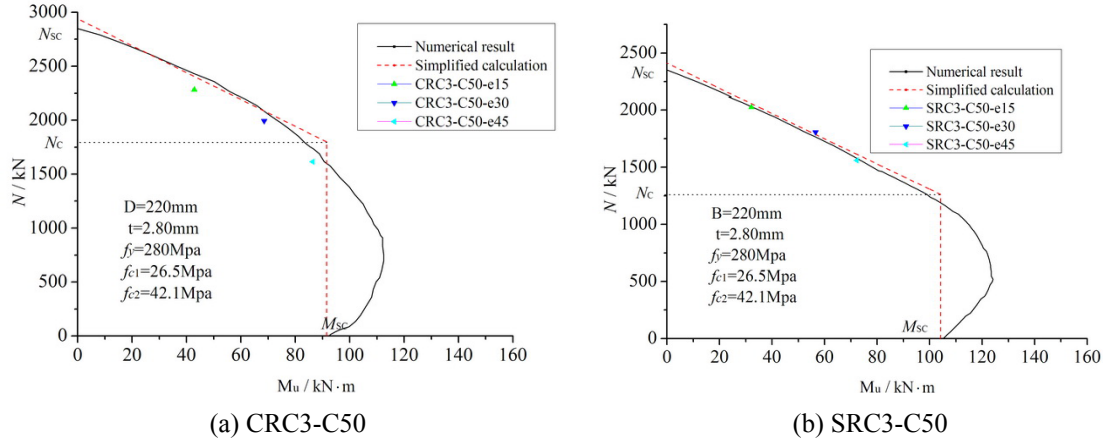
(a) CRC3-C50   (b) SRC3-C50

Fig. 12 The typical M_p-N interaction curve for the strengthened columns

Substitute Eq. (19) into Eq. (18) gives the ultimate load N_u for the eccentrically strengthened column as

$$N_u = \begin{cases} \dfrac{1}{1+a/k_1} N_{SC} & (N_u > N_C) \\ k_1 N_{SC} & (N_u \le N_C) \end{cases} \tag{22}$$

$$k_1 = \frac{2k(1+k-\sqrt{k^2+2k})M_{SC}}{N_{SC}e_0} \tag{23}$$

The experimental results are compared with the calculated results using Eq. (22) in Table 1. It can be seen from the Table 1 that the proposed design formula gives very good prediction of the ultimate loads of strengthening columns. The mean of N_{exp}/N_{pre} is 0.97 and the standard deviation of it is 0.067 while its coefficient of variation is 0.069. Therefore, it can be concluded from the comparisons that the proposed formula can predict fairly well for the ultimate eccentric strength of the strengthening columns and the axial strength of strengthening slender columns.

6. Conclusions

The experimental results of 14 RC columns strengthened with Self-compacting Concrete Filled steel Tubes (SCFT) under eccentric load are presented in this paper. It has been shown that the use of SCFT is interesting since the ductility and the bearing capacity of the RC columns are greatly improved. And the performance of the strengthened columns is significantly affected by four parameters: column section type, wall thickness of the steel tube (t), compressive strength of the strengthening concrete (f_c) and initial eccentricity. The following conclusions are reached within the scope of the current research.

● The ultimate strengths of CRC columns with smaller cross-section is approximate 12%

more than that of SRC, which indicates that the enhanced confinement provided by circular steel tube is more effective than that of square steel tube.

● The experimental results indicates that better performance of the strengthened columns can be gained by thicker steel tubes and higher strength concrete, while the wall thickness of steel tubes has a more significantly enhanced effect than concrete strength. And the ductility significantly increases with the wall thickness of steel tubes increasing, while the ductility significantly decreases with the strength increasing, especially in the use of high strength concrete.

● The initial eccentricity has a remarkably detrimental effect on ultimate strength of strengthened columns. The ultimate strength decreases considerably with an increase in the initial eccentricity. Therefore to achieve the aims of safety, the strengthened columns with large initial eccentricity are not recommended to be used in practice.

Moreover, a generic fiber element model which takes in account the effect of confinement is developed to predict the behavior of the strengthened columns subjected to eccentric loading. After the fiber element analysis were verified against experimental results, a simple design formula based on the model is proposed. Calibration of the design formula against the test results shows that it closely estimates the ultimate capacities of the strengthened columns by 5%.

Acknowledgments

References

Chang, X., Huang, C.K., Jiang, D.C. and Song, Y.C. (2009), "Push-out test of pre-stressing concrete filled circular steel tube columns by means of expansive cement", *Constr. Build. Mater.*, **23**(1), 491-497.

Elremaily, A. and Azizinamini, A. (2002), "Behavior and strength of circular concrete-filled tube columns", *J. Constr. Steel Res.*, **58**(12), 1567-1591.

Han, L.H. (2007), *Concrete-Filled Steel Tube Columns*, Science Publishing Company, Beijing, China. [In Chinese]

Holschemacher, K. (2004), "Hardened material properties of self-compacting concrete", *J. Civil Eng. Manag.*, **10**(4), 261-266.

Liang, Q.Q. (2011), "High strength circular concrete-filled steel tubular slender beam–columns, Part I: Numerical analysis", *J. Constr. Steel Res.*, **67**(2), 164-171.

Liu, D.L. (2006), "Behaviour of eccentrically loaded high-strength rectangular concrete-filled steel tubular columns", *J. Constr. Steel Res.*, **62**(8), 839-846.

Loser, R. and Leemann, A. (2009), "Shrinkage and restrained shrinkage cracking of self-compacting concrete compared to conventionally vibrated concrete", *Mater. Struct.*, **42**(1), 71-82.

Lu, F.W., Li, S.P. and Sun G. (2007), "A study on the behavior of eccentrically compressed square concrete-filled steel tube columns", *J. Constr. Steel Res.*, **63**(7), 941-948.

Lu, Y.Y., Gong, T.N., Zhang X.P. and Xue, J.F. (2013), "Experimental research on behavior of circular RC

column strengthened with self-compacting concrete filled circular steel jacket under axial loading", *J. Build. Struct*., **34**(6), 121-128. [In Chinese]

Miller, E.A. (2006), "Experimental research of reinforced concrete column strengthening methods", Master Thesis, The Ohio State University, Volume 24-30, pp. 222-230.

Muciaccia, G., Giussani, F., Rosati, G. and Mola, F. (2011), "Response of self-compacting concrete filled tubes under eccentric compression", *J. Constr. Steel Res*., **67**(5), 904-916.

Priestley, M.J.N., Seible, F., Xiao, Y. and Verma, R. (1994a), "Steel jacket retrofitting of reinforced concrete bridge columns for enhanced shear strength-part 1: Theoretical considerations and test design", *ACI*, *Struct. J*., **91**(4), 394-405.

Priestley, M.J.N., Seible, F., Xiao, Y. and Verma, R. (1994b), "Steel jacket retrofitting of reinforced concrete bridge columns for enhanced shear strength-part 2: Test results and comparison with Theory", *ACI*, *Struct. J*., **91**(5), 537-551.

Roeder, C.W., Cameron, B. and Brown, C.B. (1999), "Composite action in concrete filled tubes", *J. Struct. Eng*., *ASCE*, **125**(5), 477-484.

Sezen, H. and Miller, E.A. (2011), "Experimental evaluation of axial behavior of strengthened circular reinforced-concrete columns", *J. Bridge Eng*., *ASCE*, **16**(2), 238-247.

Wang, M.H. (2011), "Experimental study on axial-Compression reinforced concrete column strengthened by circular steel tube", *Appl. Mech. Mater*., **94**, 1261-1270.

Wang, Y., Zhou, Y.X. and Xia, Y.M. (2000), "Numerical analysis of stress concentration for brittle matrix composites", *Appl. Compos. Mater*., **7**(1), 39-49.

Zhou, M., Li, J.W. and Duan, J.M. (2012), "Experimental study on the axial loading tests of RC columns strengthened with steel tube", *Appl. Mech. Mater*., **204**, 2878-2882.

BU